International Journal of Computational Methods
Vol. 15, No. 7 (2018) 1850064 (27 pages)

DOI: 10.1142/S0219876218500640

World Scientific
www.worldscientific.com

Kriging-Based Timoshenko Beam Elements with the Discrete Shear Gap Technique

F. T. Wong*
Department of Civil Engineering, Petra Christian University
Jl. Siwalankerto 121-131, Surabaya 60236, Indonesia
**wftjong@petra.ac.id*

Adam Sulistio
Department of Civil and Construction Engineering
National Taiwan University of Science and Technology
Taipei, Taiwan
adamsulistio@gmail.com

Hidayat Syamsoeyadi
Nebethes Design, Bandung, Indonesia
hdyt87@yahoo.com

Received 23 April 2016
Accepted 28 October 2017
Published 19 December 2017

Kriging-based finite element method (K-FEM) is an enhancement of the FEM through the use of Kriging interpolation in place of the conventional polynomial interpolation. In this paper, the K-FEM is developed for static, free vibration, and buckling analyses of Timoshenko beams. The discrete shear gap technique is employed to eliminate shear locking. The numerical tests show that a Kriging-Based beam element with cubic basis and three element-layer domain of influencing nodes is free from shear locking. Exceptionally accurate displacements, bending moments, natural frequencies, and buckling loads and reasonably accurate shear force can be achieved using a relatively course mesh.

Keywords: Timoshenko beam; Kriging-based finite element; shear locking; discrete shear gap.

1. Introduction

An enhancement of the finite element method, referred to as the Kriging-based finite element method (K-FEM), was proposed by Plengkhom and Kanok-Nukulchai [2005]. In the K-FEM, Kriging interpolation (KI) is employed as the trial and test

*Corresponding author.

functions in place of a conventional polynomial function. This KI is constructed for each element from a set of nodal values within a domain of influencing nodes (DOI) comprising the element itself and several layers of the surrounding elements. The DOI is thus a polygon in the 2D domain and a polyhedron in the 3D domain. The advantages of this novel proposed method are as follows: (1) a high degree of polynomial function can be easily included in the trial function without adding any side or internal nodes to the element; (2) higher accuracy and better smoothness results for the field variables and their derivatives, in comparison to the conventional FEM, can be obtained using even the simplest form of elements; (3) furthermore, the computer implementation of the proposed method is very similar to that of conventional FEM, so an existing general FEM code can be extended to include the method without major changes.

The K-FEM [Plengkhom and Kanok-Nukulchai (2005)] was subsequently improved through the use of adaptive correlation parameters and developed for analysis of Reissner–Mindlin plates [Wong and Kanok-Nukulchai (2006a)]. A shortcoming of the K-FEM is that the resulting approximate function is discontinuous across the element boundaries, or in other words, nonconforming between interconnected elements. The issue of the nonconformity was studied in [Wong and Kanok-Nukulchai (2009b)] and it is concluded that the K-FEM with appropriate Kriging parameters always yield converging results.

In the development of the K-FEM for analyses of shear deformable beams, plates, and shells, as in the FEM, the difficulty of shear locking also occurs. In attempts to overcome this difficulty, the field-matching technique of Kanok-Nukulchai *et al.* [2001], which works well in the element-free Galerkin method [Belytschko *et al.* (1994)], has been employed [Wong (2009)]. Using this technique, the shape functions for the rotational fields are taken as the derivatives of the shape functions for the deflection. It is found that the K-FEM with the field-matching strategy yields erroneous results. Accordingly, the field-matching technique is not applicable in the framework of the K-FEM. Another attempt is the introduction of assumed natural transverse shear strains in the K-FEM [Wong and Kanok-Nukulchai (2006b)]. This study discovers that the assumed shear strain method can relieve the locking but cannot eliminate it completely because the locations of shear-strain sampling points in the K-FEM cannot be determined exactly. Henceforth, a basis function of sufficiently high degree (cubic or higher) in the K-FEM for analyses of plates and shell structures is employed as a provisional solution to relieve the shear locking [Wong and Kanok-Nukulchai (2006a, 2008, 2009b); Wong (2009, 2013); Wong *et al.* (2015)]. The use of a high-degree polynomial basis, however, cannot completely eliminate the locking and makes the computational cost high. Thus, it is essential to have an effective method to eliminate shear locking in the K-FEM.

To develop a locking-free formulation for the K-FEM for analyses of plates and shells, it is instructive to study the K-FEM in the simpler problem of the Timoshenko beam model in order to gain understanding and insight about a locking-free

device. In this spirit, Wong and Syamsoeyadi [2011] developed the K-FEM for static and free vibration analyses of Timoshenko beams. In this work, the shear locking is eliminated using the well-known selective-reduced integration (SRI) technique. While the SRI technique can effectively eliminate shear locking, it deteriorates the accuracy in the case of thick beams and also worsens the shear force results [Wong and Syamsoeyadi (2011)]. Moreover, it has been proved that the SRI technique is not applicable to a Kriging-based triangular plate bending element [Wong (2009)]. Therefore, a new shear-locking-elimination technique that is extendable to a Kriging-based Reissner–Mindlin plate element needs to be explored.

Bletzinger *et al.* [2000] presented a unified approach to eliminate shear locking in shear deformable plates and shells, called the discrete shear gap (DSG) technique. In this approach, the shear gap is defined as the difference between the total deflection and the bending deflection, or in other words, it is the deflection corresponding to the shear strain. The shear gap is calculated at the element nodes (called the *discrete* shear gaps) and interpolated across the element domain. The substitute shear strain is then obtained from the derivatives of the interpolated discrete shear gaps. With this technique, a locking-free formulation of plate elements, either triangular or rectangular of any polynomial degree, can be carried out in a simple way. The technique was subsequently generalized to a more general concept applicable to other locking problems such as membrane locking [Bischoff *et al.* (2003); Koschnick *et al.* (2005)].

The DSG technique has been applied not only in the conventional FEM but also in recent alternative computational methods such as the edge-based smoothed FEM [Nguyen-Xuan *et al.* (2010a)] and node-based smoothed FEM [Nguyen-Xuan *et al.* (2010b)]. The most recent application of the DSG approach is to combine the DSG three-node triangular element with the cell-based smoothed FEM to produce a three-node triangular plate element, which is claimed to have some superior properties compared to many existing plate elements of the same class [Nguyen-Thoi *et al.* (2012, 2015)]. These recent and successful applications of the DSG technique suggest that it may also be effective at eliminating shear locking in Kriging-based shear deformable beams, plates, and shells.

The aim of this paper is to present the development and testing of the K-FEM with the DSG technique for static, free vibration, and buckling analyses of Timoshenko beams. The discretized equations are formulated using the standard displacement-based finite element procedure on the variational form. The same Kriging shape functions are used for the deflection and rotation variables. To apply the DSG technique, the discrete shear gaps at all nodes in a DOI under consideration are evaluated from the integration of the kinematic shear strain. The DSG shear strain is then calculated from the derivative of the Kriging-based interpolated discrete shear gaps. The original displacement-based transverse shear strain is replaced with the DSG shear strain to eliminate the shear locking. A series of numerical tests in static, free vibration, and buckling problems are carried

out to evaluate the accuracy and convergence of the Kriging-based Timoshenko beam element. Special attention is given to numerical investigation of the shear locking.

It is worth mentioning here that although some researchers have employed the DSG technique with a stabilization parameter α to improve the accuracy and stability against mesh distortion [Bischoff *et al.* (2003); Nguyen-Thoi *et al.* (2012); Nguyen-Xuan *et al.* (2010a, 2010b)], we do not resort to this approach because the parameter α is problem dependent and makes the role of the shear correction factor obscure.

2. Kriging Interpolation in the K-FEM

Named after Danie G. Krige, a South African mining engineer, Kriging is a well-known geostatistical technique for spatial data interpolation in geology and mining (see, e.g., geostatistics texts [Olea (1999); Wackernagel (2003)]. Reviews of KI in the framework of the K-FEM have been published in several previous papers [Wong and Kanok-Nukulchai (2009a, 2009b); Wong and Syamsoeyadi (2011)]. In this paper only the key points of KI that are necessary for the subsequent development are addressed.

2.1. *Kriging shape function*

We consider a one-dimensional problem domain Ω where a continuous field variable (a scalar function) $u(x)$ is defined. The domain is represented by a set of properly scattered nodes x_I, $I = 1, 2, \ldots, N$, where N is the total number of nodes in the whole domain. Given N field values $u(x_1), \ldots, u(x_N)$, the problem of interest is to obtain an estimated value of u^{h} at a point $x \,\epsilon\, \Omega$.

In the Kriging method, the unknown value $u^{\mathrm{h}}(x)$ is estimated from a linear combination of the field values at the neighboring nodes, that is,

$$u^{\mathrm{h}}(x) = \sum_{i=1}^{n} \lambda_i(x) u(x_i), \tag{1}$$

where the $\lambda_i(x)$'s are the unknown *Kriging weights* and n is the number of nodes surrounding point x inside and on the boundary of a subdomain $\Omega_x \subseteq \Omega$, $n \leq N$. Here, small letters i and n are used instead of I and N to signify that the numbering is referred to the local (subdomain) numbering system.

In the context of the K-FEM [Wong and Kanok-Nukulchai (2009a, 2009b); Wong and Syamsoeyadi (2011)], the nodes are identical to finite element nodes and the weights are identical to shape functions. Furthermore, the subdomain Ω_x in the K-FEM is composed of the element of interest and several layers of surrounding elements and referred to as the DOI. The number of element layers of the DOI can be one, two, or more. In the case of one layer, the DOI is the finite element itself and the K-FEM becomes identical to the conventional FEM. Figure 1 illustrates a two-layer DOI encompassing local nodes 1–4.

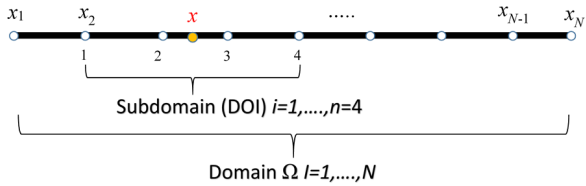

Fig. 1. One-dimensional domain and a two element-layer subdomain.

The Kriging weights $\lambda_i(x)$, $i = 1, \ldots, n$, are obtained by solving the Kriging equation system:

$$\mathbf{R}\boldsymbol{\lambda}(x) + \mathbf{P}\boldsymbol{\mu}(x) = \mathbf{r}(x), \tag{2a}$$

$$\mathbf{P}^{\mathrm{T}}\boldsymbol{\lambda}(x) = \mathbf{p}(x), \tag{2b}$$

in which

$$\mathbf{R} = \begin{bmatrix} C(h_{11}) & \cdots & C(h_{1n}) \\ \cdots & \cdots & \cdots \\ C(h_{n1}) & \cdots & C(h_{nn}) \end{bmatrix}; \quad \mathbf{P} = \begin{bmatrix} p_1(x_1) & \cdots & p_m(x_1) \\ \cdots & \cdots & \cdots \\ p_1(x_n) & \cdots & p_m(x_n) \end{bmatrix}, \tag{2c}$$

$$\boldsymbol{\lambda}(x) = [\lambda_1(x) \cdots \lambda_n(x)]^{\mathrm{T}}; \quad \boldsymbol{\mu}(x) = [\mu_1(x) \cdots \mu_m(x)]^{\mathrm{T}}, \tag{2d}$$

$$\mathbf{r}(x) = [C(h_{1x})\ C(h_{2x}) \cdots C(h_{nx})]^{\mathrm{T}}; \quad \mathbf{p}(x) = [p_1(x) \cdots p_m(x)]^{\mathrm{T}}. \tag{2e}$$

Each entry in matrix $\mathbf{R}$, $C(h_{ij})$, is the covariance between $U(x_i)$ and $U(x_j)$, which is a function of $h_{ij} = x_j - x_i$; $i = 1, \ldots, n$; $j = 1, \ldots, n$. Thus, $\mathbf{R}$ is the $n \times n$ matrix of the covariance of $U(x)$ at nodes in the DOI, $x_1, \ldots, x_n$. The capital '$U(x)$' here signifies the corresponding random process of the deterministic function $u(x)$. Matrix $\mathbf{P}$ is the $n \times m$ matrix of monomial values at the nodes, where m is the number of monomial terms. Vector $\boldsymbol{\lambda}(x)$ is the unknown $n \times 1$ vector of Kriging weights and vector $\boldsymbol{\mu}(x)$ is the unknown $m \times 1$ vector of Lagrange multipliers. On the right hand side of Eqs. (2a) and (2b), vector $\mathbf{r}(x)$ is the $n \times 1$ vector of covariance between the nodes and the point of interest, x, and $\mathbf{p}(x)$ is the $m \times 1$ vector of monomial values at x. Each entry in $\mathbf{r}(x)$, $C(h_{ix})$, is the covariance between $U(x_i)$ and $U(x)$, which is a function of $h_{ix} = x - x_i$. A necessary condition to make the Kriging equation system solvable (nonsingular) is that the number of nodes in the DOI, n, should be equal to or greater than the number of monomial terms, m, that is, $n \geq m$.

Solving the Kriging equation system, the vector of Kriging weights is given as

$$\boldsymbol{\lambda}^{\mathrm{T}}(x) = \mathbf{p}^{\mathrm{T}}(x)\mathbf{A} + \mathbf{r}^{\mathrm{T}}(x)\mathbf{B}, \tag{3a}$$

where

$$\mathbf{A} = (\mathbf{P}^{\mathrm{T}}\mathbf{R}^{-1}\mathbf{P})^{-1}\mathbf{P}^{\mathrm{T}}\mathbf{R}^{-1}, \quad \mathbf{B} = \mathbf{R}^{-1}(\mathbf{I} - \mathbf{P}\mathbf{A}). \tag{3b}$$

Here, $\mathbf{A}$ is an $m \times n$ matrix, $\mathbf{B}$ is an $n \times n$ matrix, and $\mathbf{I}$ is the $n \times n$ identity matrix.

The expression for the estimated value u^{h}, Eq. (1), can be restated in matrix form as

$$u^{\mathrm{h}}(x) = \boldsymbol{\lambda}^{\mathrm{T}}(x)\mathbf{d} = \mathbf{N}(x)\mathbf{d}, \tag{4}$$

where $\mathbf{d} = [u(x_1), \ldots, u(x_n)]^{\mathrm{T}}$ is an $n \times 1$ vector of nodal values and $\mathbf{N}(x) = \boldsymbol{\lambda}^{\mathrm{T}}(x)$ is the matrix of Kriging shape functions. It is obvious that the Kriging weights are nothing but the shape functions.

2.2. *Polynomial basis and correlation function*

In order to construct Kriging shape functions, a polynomial basis function and a covariance function should be chosen. In the present research, as in the previous research on the K-FEM for analysis of Timoshenko beams [Wong and Syamsoeyadi (2011)], polynomial bases of degree one to three are employed. The higher the polynomial degree, the more element layers are needed in the DOI because of the requirement that $n \geq m$. The minimum number of DOI layers for different polynomial bases is listed in Table 1.

The covariance $C(h)$ is more conveniently expressed in terms of a correlation function, which is given as

$$\rho(h) = \frac{C(h)}{\sigma^2}, \tag{5}$$

where h is the distance between points x and $x + h$, and σ^2 is the variance of the random function $U(x)$. The variance σ^2 has no effect on the resulting Kriging shape functions and is taken to be equal to 1 in this study. There are many possibilities for the correlation function model in the area of geostatistics [Olea (1999); Wackernagel (2003)], such as the Nugget-effect model, exponential model, and spherical model. In the present study, as in the previous research [Wong and Syamsoeyadi (2011)], the Gaussian correlation function, that is,

$$\rho(h) = \exp\left(-\left(\theta_r \frac{h}{d}\right)^2\right), \tag{6}$$

and the quartic spline (QS), that is,

$$\rho(h) = \begin{cases} 1 - 6\left(\theta_r \dfrac{h}{d}\right)^2 + 8\left(\theta_r \dfrac{h}{d}\right)^3 - 3\left(\theta_r \dfrac{h}{d}\right)^4 & \text{for } 0 \leq \theta_r \dfrac{h}{d} \leq 1 \\ 0 & \text{for } \theta_r \dfrac{h}{d} > 1 \end{cases}, \tag{7}$$

Table 1. Minimum number of layers for different polynomial bases.

Polynomial basis	Monomial terms	m	Minimum number of layers
Linear	$1\ x$	2	1
Quadratic	$1\ x\ x^2$	3	2
Cubic	$1\ x\ x^2\ x^3$	4	3

are chosen. In these equations, $\theta_r > 0$ is the correlation parameter and d is a scale factor to normalize the distance h. Factor d is taken to be the largest distance between any pair of nodes in the DOI.

The parameter θ_r is an important parameter affecting the validity of Kriging shape functions. Too small a value of θ_r deteriorates the partition of unity property of the shape functions [Plengkhom and Kanok-Nukulchai (2005)], that is,

$$\left| \sum_{i=1}^{n} N_i - 1 \right| \neq 1. \tag{8}$$

Conversely, too large a value of θ_r may make the Kriging equation system singular. Based on these facts, Plengkhom and Kanok-Nukulchai [2005] proposed a rule of thumb for the lower and upper bounds of θ_r. Following this rule, the value of θ_r should be selected so that it satisfies the lower bound criterion

$$\left| \sum_{i=1}^{n} N_i - 1 \right| \leq 1 \times 10^{-10+a}, \tag{9}$$

where a is the degree of the basis function, and the upper bound criterion

$$\det(\mathbf{R}) \leq 1 \times 10^{-b}, \tag{10}$$

where b is the dimension of the problem. For the 1D problem and quadratic basis function, for example, $a = 2$ and $b = 1$.

The range of appropriate values of θ_r varies with the number of monomial terms m, the number of the nodes in the DOI, n, and the correlation model used [Plengkhom and Kanok-Nukulchai (2005); Wong and Kanok-Nukulchai (2006a)]. In other words, it depends on the polynomial basis, the number of element layers, and the type of correlation function employed in the analysis. The range of θ_r for 1D problems satisfying the lower and upper bound criteria, Eqs. (9) and (10), has been numerically examined [Wong and Syamsoeyadi (2011)] and the results are presented in Table 2. It is recommended that the mid-value between the upper and lower bounds be taken to ensure good quality of the KI.

Table 2. The lower and upper bounds of θ_r for 1D problems.

		Gaussian $\rho(h)$		Quartic spline $\rho(h)$	
Polynomial basis	Number of layers	Lower bound	Upper bound	Lower bound	Upper bound
Linear	1	0	0.2295	0	0.098
	2	10^{-4}	1.0	10^{-5}	0.44
	3	10^{-4}	1.9	10^{-5}	0.86
Quadratic	2	10^{-4}	1.0	10^{-5}	0.44
	3	10^{-4}	1.9	10^{-6}	0.86
Cubic	3	10^{-4}	1.9	10^{-8}	0.86

3. Formulation of Kriging-Based Timoshenko Beam Element

We consider a beam of length L with cross-sectional area and moment of inertia A and I, respectively. The beam is made from a homogeneous and isotropic material with modulus of elasticity E, shear modulus G, and mass density ρ (per unit volume). A Cartesian coordinate system (x, y, z) is established, where the x-axis coincides with the neutral axis and the y and z-axes coincide with the principal axes of the cross-section (Fig. 2). The beam is subjected to a dynamic distributed transversal load $q = q(x, t)$ and a distributed moment $m = m(x, t)$, $0 \leq x \leq L$, $t \geq 0$. In the Timoshenko beam theory, the motion of the beam due to external loads is described using two independent field variables, namely the transverse displacement (deflection) of the neutral axis $w = w(x, t)$ and the rotation of the cross-section $\theta = \theta(x, t)$. The sign convention for these variables is shown in Fig. 2.

To account for the effect of axial force on the deflection, let the beam be also subjected to an axial force $P = P(t)$ at the end of the beam. The sign of P is positive when it is a tensile force. This axial force is imposed at the outset, for example by a pre-stressed cable system. The deflection is assumed to be small so that the axial force P remains essentially constant. In addition, the beam is assumed to be initially, perfectly straight so that the coupling between bending and membrane deformations can be neglected. Thus, the present Timoshenko beam model is a linear-elastic model enhanced with a nonlinear Green strain term for the axial strain [Cook *et al.* (2002), Ch. 18]. This model can be reduced to the bifurcation buckling model by removing the transversal load q and external moment m and assuming that the axial force P is an unknown.

The governing equation for the motion of the beam at time t, including the axial load effect, can be expressed in a variational form as

$$\begin{aligned}\int_0^L \delta w \rho A \ddot{w}\, dx + \int_0^L \delta\theta \rho I \ddot{\theta}\, dx \\ + \int_0^L \delta\theta_{,x}\, EI\theta_{,x}\ dx + \int_0^L \delta\gamma GA_s\gamma\, dx + \int_0^L \delta w_{,x}\, P w_{,x}\ dx \\ = \int_0^L \delta w q\, dx + \int_0^L \delta\theta m\, dx. \end{aligned} \tag{11}$$

In this equation,

$$\gamma = w_{,x} - \theta, \tag{12}$$

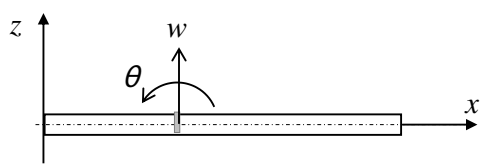

Fig. 2. Coordinate system and positive directions for the deflection and rotation.

is the transverse shear strain and $A_S = kA$ is the effective shear area, where k is a shear correction factor that is dependent upon the cross-section geometry. The double dots signify the second partial derivative of the corresponding variable with respect to the time variable t, while the comma signifies the first partial derivative of it with respect to the variable next to it (i.e., x). The operator δ signifies the variational operation on the corresponding variable. A detailed derivation of the variational equation, Eq. (11), using Hamilton's principle is given in Friedman and Kosmatka [1993] and Kosmatka [1995].

The bending moment and shear force along the beam can be calculated from the deflection w and rotation θ as follows:

$$M = EI\theta_{,x}\,, \tag{13}$$

$$Q = GA_s(w_{,x} - \theta) + Pw_{,x}\,. \tag{14}$$

To obtain an approximate solution using the concept of KI with a layered-element DOI, the beam is subdivided into Nel elements and N nodes. We then consider an element with a DOI that contains n nodes, as illustrated in Fig. 3. The field variables w and θ over the element are approximated using KI as follows:

$$w = \mathbf{N}_w(x)\mathbf{d}(t), \tag{15a}$$

$$\theta = \mathbf{N}_\theta(x)\mathbf{d}(t), \tag{15b}$$

where

$$\mathbf{N}_w(x) = [N_1(x) \quad 0 \quad N_2(x) \quad 0 \quad \ldots \quad N_n(x) \quad 0], \tag{15c}$$

$$\mathbf{N}_\theta(x) = [0 \quad N_1(x) \quad 0 \quad N_2(x) \quad \ldots \quad 0 \quad N_n(x)], \tag{15d}$$

are the matrices of Kriging shape functions for the deflection and rotation, respectively, and

$$\mathbf{d}(t) = [w_1(t) \quad \theta_1(t) \quad w_2(t) \quad \theta_2(t) \quad \ldots \quad w_n(t) \quad \theta_n(t)]^{\mathrm{T}}, \tag{15e}$$

is the vector of nodal displacement. The variable x here refers to the local (element) coordinate system. The number of nodes, n, depends on the number of elements

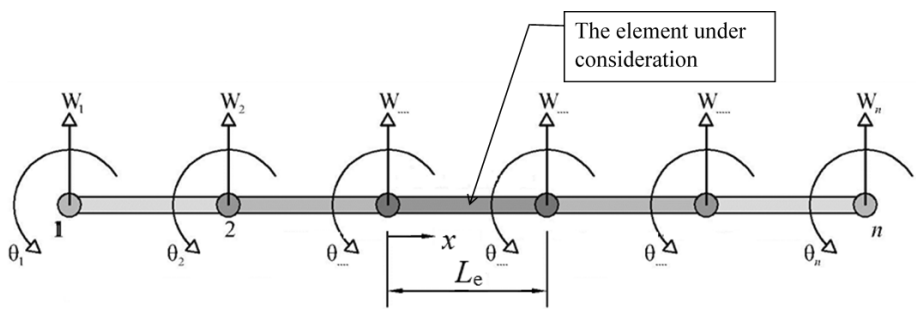

Fig. 3. A typical beam element and its domain of influencing nodes (DOI).

used in the DOI and differs for the interior and exterior elements. For example, for an element with a two-layer DOI, $n = 3$ for the exterior element and $n = 4$ for the interior element.

Substituting Eqs. (15a) and (15b) into Eq. (11) and carrying out the standard finite element formulation yield the discretized system of equations

$$\mathbf{m}\ddot{\mathbf{d}}(t) + (\mathbf{k} + P\mathbf{k}_g)\mathbf{d}(t) = \mathbf{f}(t). \tag{16}$$

In this equation,

$$\mathbf{m} = \int_0^{L_e} \mathbf{N}_w^{\mathrm{T}} \rho A \mathbf{N}_w dx + \int_0^{L_e} \mathbf{N}_\theta^{\mathrm{T}} \rho I \mathbf{N}_\theta dx \tag{17}$$

is the element consistent mass matrix,

$$\mathbf{k} = \int_0^{L_e} \mathbf{B}_\theta^{\mathrm{T}} EI \mathbf{B}_\theta dx + \int_0^{L_e} \mathbf{B}_\gamma^{\mathrm{T}} GA_s \mathbf{B}_\gamma dx \tag{18}$$

is the element stiffness matrix,

$$\mathbf{k}_g = \int_0^{L_e} \mathbf{B}_w^{\mathrm{T}} \mathbf{B}_w dx \tag{19}$$

is the element geometrical stiffness matrix, and

$$\mathbf{f}(t) = \int_0^{L_e} \mathbf{N}_w^{\mathrm{T}} q dx + \int_0^{L_e} \mathbf{N}_\theta^{\mathrm{T}} m dx \tag{20}$$

is the element equivalent nodal force vector. The order of all square matrices and vectors is $2n$. In Eqs. (18) and (19), matrices $\mathbf{B}_\theta$, $\mathbf{B}_w$, and $\mathbf{B}_\gamma$ are defined as follows:

$$\mathbf{B}_\theta = \frac{d}{dx}\mathbf{N}_\theta, \quad \mathbf{B}_w = \frac{d}{dx}\mathbf{N}_w, \tag{21a}$$

$$\mathbf{B}_\gamma = \mathbf{B}_w - \mathbf{N}_\theta. \tag{21b}$$

The unknowns of Eq. (16) are the element nodal acceleration vector $\ddot{\mathbf{d}}(t)$ and the nodal displacement vector $\mathbf{d}(t)$.

The discretized equations for static, free vibration, and buckling problems can be obtained from Eq. (16) by simply reducing it, respectively, to

$$\mathbf{k}\mathbf{d} = \mathbf{f}, \tag{22}$$

$$\mathbf{m}\ddot{\mathbf{d}}(t) + \mathbf{k}\mathbf{d}(t) = \mathbf{0}, \tag{23}$$

$$(\mathbf{k} + P\mathbf{k}_g)\mathbf{d} = \mathbf{0}. \tag{24}$$

The corresponding global discretized equations of these equations can be obtained using the finite element assembly procedure. It should be mentioned here that the assembly process involves all nodes in the DOI, not just the element nodes as in the conventional FEM.

4. Application of the Discrete Shear Gap Concept

It is well known that the pure displacement-based formulation of a Timoshenko beam (with exact integration of all integrals) leads to the shear locking phenomenon in the FEM [Bathe (1996); Cook *et al.* (2002); Hughes (1987); Liu and Quek (2003); Prathap (1993, 2001); Reddy (2006)]. The same is true for a Kriging-based Timoshenko beam element [Wong and Syamsoeyadi (2011)], even for an element with a cubic polynomial basis function. The primary cause of this locking is the inability of the approximate shear strain to vanish as the beam becomes extremely thin. The basic idea of the DSG concept [Bischoff *et al.* (2003); Bletzinger *et al.* (2000)] is to replace the troublesome kinematic shear strain with a substitute shear strain field determined from the derivative of interpolated discrete shear gaps. This section presents a review of the DSG concept and its application to Timoshenko beam elements with KI.

To apply the DSG concept, we begin with the definition of *shear gap*, that is,

$$\Delta w_\gamma(x) = \int_{x_0}^{x} \gamma dx, \tag{25}$$

where $\Delta w_\gamma(x)$ is the shear gap at point x, and x_0 is the position of a chosen reference point. Inserting Eq. (12) into this equation results in

$$\Delta w_\gamma(x) = w|_{x_0}^{x} - \int_{x_0}^{x} \theta dx, \tag{26a}$$

$$\Delta w_\gamma(x) = (w(x) - w(x_0)) - \int_{x_0}^{x} \theta dx = \Delta w(x) - \Delta w_b(x). \tag{26b}$$

In these equations, Δw is the increase of the actual deflection between the positions x and x_0, and Δw_b is the increase of the deflection due to bending action. The shear gap Δw_γ thus represents the increase of the deflection due to shearing action.

The DSG at a finite element node with position x_i, $\Delta w_{\gamma i}$ is defined as

$$\Delta w_{\gamma i} = \Delta w_\gamma(x_i) = w|_{x_0}^{x_i} - \int_{x_0}^{x_i} \theta dx. \tag{27}$$

A modified shear gap field is defined as the interpolation of the nodal shear gaps, that is,

$$\Delta \bar{w}_\gamma(x) = \sum_{i=1}^{n} N_i(x) \Delta w_{\gamma i}. \tag{28}$$

In the framework of the standard FEM, n is the number of number of nodes in the element and $Ni(x)$, $i = 1, \ldots, n$ are the shape functions. In the present research, however, n is the number of nodes in the DOI and $Ni(x)$ are Kriging shape functions. Differentiating Eq. (28) gives the *substitute* shear strain, that is,

$$\bar{\gamma}(x) = \sum_{i=1}^{n} N_{i,x} \Delta w_{\gamma i} = \bar{\mathbf{B}}_{\gamma 1} \mathbf{w}_\gamma, \tag{29a}$$

where

$$\bar{\mathbf{B}}_{\gamma 1} = [N_{1,x} \quad N_{2,x} \quad \ldots \quad N_{n,x}], \tag{29b}$$

$$\mathbf{w}_{\gamma} = [\Delta w_{\gamma 1} \quad \Delta w_{\gamma 2} \quad \ldots \quad \Delta w_{\gamma n}]^{\mathrm{T}}. \tag{29c}$$

To avoid the shear locking problem, the kinematic shear strain γ, Eq. (12), is replaced with $\bar{\gamma}$, Eq. (29a). In order to implement this technique for the Kriging-based beam elements, we first need to express the nodal shear gaps in the DOI, $\mathbf{w}_{\gamma}$, in terms of the degrees of freedom of the Timoshenko beam. Choosing node 1 as the reference point (see Fig. 3) and inserting Eq. (15b) into Eq. (27), the discrete shear gaps are given as

$$\Delta w_{\gamma i} = w_i - w_1 - \left(\int_{x_1}^{x_i} \mathbf{N}_{\theta}(x) dx \right) \mathbf{d}. \tag{30}$$

Evaluating the discrete shear gaps for nodes 1 to n and writing them in matrix form, the discrete shear gaps for all nodes in the DOI can be expressed as

$$\mathbf{w}_{\gamma} = \bar{\mathbf{B}}_{\gamma 2} \mathbf{d}, \tag{31a}$$

where

$$\bar{\mathbf{B}}_{\gamma 2} = \begin{bmatrix} 0 & 0 & 0 & 0 & 0 & 0 & \cdots & 0 & 0 \\ -1 & -\int_{x_1}^{x_2} N_1 dx & 1 & -\int_{x_1}^{x_2} N_2 dx & 0 & -\int_{x_1}^{x_2} N_3 dx & \cdots & 0 & -\int_{x_1}^{x_2} N_n dx \\ -1 & -\int_{x_1}^{x_3} N_1 dx & 0 & -\int_{x_1}^{x_3} N_2 dx & 1 & -\int_{x_1}^{x_3} N_3 dx & \cdots & 0 & -\int_{x_1}^{x_3} N_n dx \\ \vdots & \vdots & \vdots & \vdots & \vdots & \vdots & \vdots & \vdots & \vdots \\ -1 & -\int_{x_1}^{x_n} N_1 dx & 0 & -\int_{x_1}^{x_n} N_2 dx & 0 & -\int_{x_1}^{x_n} N_3 dx & \cdots & 1 & -\int_{x_1}^{x_n} N_n dx \end{bmatrix}. \tag{31b}$$

Substituting Eq. (31a) into Eq. (29a) yields

$$\bar{\gamma}(x) = \bar{\mathbf{B}}_{\gamma 1} \bar{\mathbf{B}}_{\gamma 2} \mathbf{d} = \bar{\mathbf{B}}_{\gamma} \mathbf{d}. \tag{32}$$

The implementation of the DSG concept is accomplished by replacing matrix $\mathbf{B}_{\gamma}$ in the expression for the element stiffness matrix, Eq. (18), with matrix $\bar{\mathbf{B}}_{\gamma}$ as defined in Eq. (32). The Kriging-based Timoshenko beam elements with the DSG shear strains are hereafter referred to as the K-beam-DSG elements.

5. Numerical Results

A series of numerical tests were carried out to evaluate: (1) the effectiveness of the DSG technique in eliminating the shear locking and (2) the accuracy and convergence characteristics of the K-beam-DSG elements with different K-FEM options

in static, free vibration, and buckling analyses. The K-FEM options used comprised of linear to cubic basis functions with one to three element-layer DOIs, and the Gaussian, Eq. (6), or quartic spline (QS), Eq. (7), correlation functions with the mid-value correlation parameters between the lower and upper bound values (Table 2). Abbreviations of the form P*-*-G or P*-*-QS were used to denote different K-FEM options. The first asterisk represents the polynomial basis, while the second represents the number of DOI element layers. The last letter or letters represent the Gaussian (G) or QS correlation function. For example, the abbreviation P2-3-QS means the K-FEM options of a quadratic basis function, three element layers, and a QS correlation function (with a mid-value correlation parameter).

In all tests, three Gaussian sampling points were employed to evaluate the integrations in the element stiffness matrix equations, Eq. (18), while two sampling points were used to evaluate the integration in the element consistent nodal load vector, Eq. (20), and $\bar{\mathbf{B}}_{\gamma 2}$, Eq. (31b). The abovementioned numbers of sampling points were chosen because we found by trial and error that they could provide accurate results with the minimum computational cost. In addition, in all tests, the shear correction factor employed was given as [Cowper (1966) as cited in Friedman and Kosmatka (1993); Kosmatka (1995)]:

$$k = \frac{10(1+\nu)}{12+11\nu}. \tag{33}$$

5.1. *Static analysis*

5.1.1. *Pure bending test*

A cantilever beam of rectangular cross-section $b \times h$ modeled with meshes of regular and irregular node distributions is shown in Fig. 4. The beam is in pure bending state with constant bending moment, M, and zero shear force along the beam. This problem is a simple test involving linear rotation and quadratic displacement fields.

The beam was analyzed using the K-beam-DSG with different polynomial bases, numbers of layers, and correlation functions. Numerical values used in the analyses were $L = 10\,\text{m}$, $b = 2\,\text{m}$, $E = 2{,}000\,\text{kN/m}^2$, $\nu = 0.3$, and $M = 1\,\text{kN-m}$. Two different length-to-thickness ratios were considered. One was moderately thick, that is, $L/h = 5$, and the other was extremely thin, that is, $L/h = 10{,}000$. The resulting deflections and rotations at the free end, w_L and θ_L, were observed and then

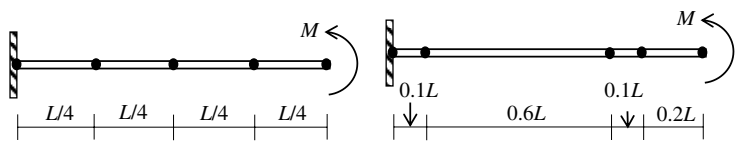

(a) Regular node distribution (b) Irregular node distribution

Fig. 4. Cantilever beam modeled with (a) regular and (b) irregular node distributions.

normalized to the corresponding exact solutions, that is,

$$w_{L\text{exact}} = \frac{ML^2}{2EI}, \quad \theta_{L\text{exact}} = \frac{ML}{EI}. \tag{34a,b}$$

The resulting bending moments and shear forces at the clamped end, calculated using Eqs. (13) and (14), were observed as well. The bending moments were then normalized to the exact bending moment, M. The shear forces, however, were not normalized because of the zero exact shear force.

The results showed that the K-beam-DSG produced values of the deflection, rotation, and bending moment with at least seven-digit accuracy (nearly exact values) for both thick and thin beams with regular node distribution. The maximum error for the shear force, however, was of the order of 10^{-5} (for the case of the thin beam analyzed using the P1-3-G option). Very accurate results for the deflection, rotation, and bending moment of the thick and thin beams were also obtained for the case of irregular node distribution, with an accuracy of at least five digits (for the thin beam analyzed using the P1-3-G option). Table 3 tabularizes the results for the most critical case, that is, the thin beam modeled with an irregular node distribution. It was seen that in this case, the accuracy of the shear force (the maximum error is of the order of 10^{-2}) was lower than that of the thin beam modeled with regular node distribution. It is worth mentioning here that the standard finite element and Kriging-based Timoshenko beam elements with selective reduced integration are unable to produce correct values for the shear force computed using Eq. (14) [Prathap (1993); Wong and Syamsoeyadi (2011)].

Overall, the results indicate that the K-beam-DSG with different analysis options virtually reproduce the exact solutions. The K-beam-DSG elements with the Gaussian correlation function generally produce less accurate results than those with the QS. In this simple problem, there is no indication of shear locking.

Table 3. Analysis results for the extremely thin cantilever beam modeled with an irregular node distribution using various K-beam-DSG options.

K-beam-DSG options	$w_L/w_{L\text{ exact}}$	$\theta_L/\theta_{L\text{ exact}}$	$M_0/M_{0\text{ exact}}$	V_0
P1-1-QS	1.0000000	1.0000000	0.9999999	$-5.36E$-09
P1-2-QS	0.9999997	0.9999997	0.9999997	$4.93E$-05
P1-3-QS	1.0000000	1.0000000	1.0000000	$-2.02E$-05
P2-2-QS	1.0000000	1.0000001	1.0000000	$-9.21E$-07
P2-3-QS	0.9999999	0.9999999	0.9999998	$3.41E$-06
P3-3-QS	1.0000001	1.0000001	1.0000002	$-1.12E$-07
P1-1-G	1.0000000	1.0000000	0.9999999	$-8.61E$-09
P1-2-G	1.0000000	0.9999998	1.0000004	$2.64E$-03
P1-3-G	1.0000056	1.0000006	1.0000367	$-6.28E$-02
P2-2-G	0.9999999	0.9999999	0.9999999	$2.71E$-03
P2-3-G	0.9999991	0.9999994	0.9999990	$-9.55E$-03
P3-3-G	1.0000002	1.0000001	1.0000005	$9.21E$-03

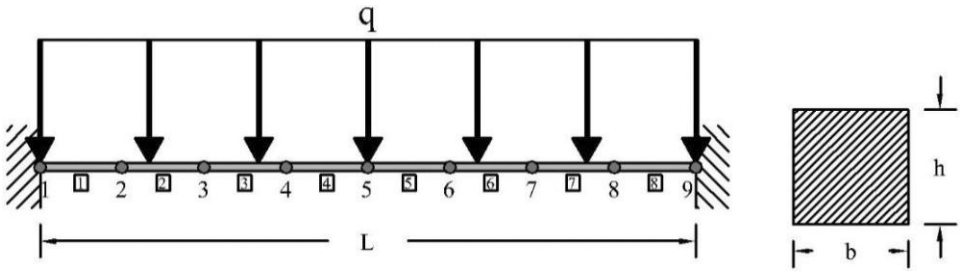

Fig. 5. Clamped–clamped beam modeled with mesh of eight elements.

5.1.2. *Investigation of shear locking*

To investigate the effectiveness of the DSG technique in eliminating shear locking, we considered a clamped–clamped beam with the finite element model as shown in Fig. 5. The height of the beam was varied from moderately thick, $L/h = 5$, to extremely thin, $L/h = 10^4$. The geometrical and material properties of the beam were the same as in the previous test (Sec. 5.1.1) with a distributed load of $q = 1\,\text{kN/m}$. The beam was analyzed using K-beam-DSG elements with different K-FEM options. The resulting deflections of the beam mid-span were observed and normalized to the exact solution, that is,

$$w_{\text{exact}} = \frac{qL^4}{384EI} + \frac{qL^2}{8GA_s}. \tag{35}$$

The results are presented in Table 4. Only the results obtained from the use of K-beam-DSG with the QS correlation function are reported here to save space. The corresponding results with the Gaussian correlation function have similar locking behavior.

It can be seen from Table 4 that for moderately thick to thin beams (i.e., $L/h = 5$ to 100), all K-beam-DSG options could produce accurate results. However, when the beam becomes thinner, it is apparent that only the K-beam-DSG elements with P1-1-QS and P3-3-QS options show no locking. Further testing of the P1-1-QS and P3-3-QS options with length-to-thickness ratios L/h greater than 10^4 reveals that there is indeed no locking up to $L/h = 10^7$. For L/h over 10^7, the results become

Table 4. Normalized deflections of the beam mid-span using various K-beam-DSG options.

K-beam-DSG options	$L/h = 5$	$L/h = 10$	$L/h = 100$	$L/h = 1{,}000$	$L/h = 10{,}000$
P1-1-QS	0.958	0.944	0.938	0.938	0.938
P1-2-QS	0.999	1.000	0.959	0.206	0.003
P1-3-QS	0.997	0.996	0.983	0.517	0.012
P2-2-QS	1.001	1.001	0.993	0.540	0.011
P2-3-QS	1.003	1.003	0.994	0.505	0.010
P3-3-QS	1.001	1.001	1.001	1.001	1.001

inaccurate because of the ill-conditioned stiffness matrix. It is worth noting that K-beam-DSG P1-1-QS is actually identical to the locking-free linear Timoshenko beam element with DSG presented in [Bischoff *et al.* (2003); Bletzinger *et al.* (2000)].

To further investigate why the shear locking phenomenon remains in the K-beam-DSG elements with linear (except with one layer) and quadratic basis functions, we considered the shear forces calculated using the 'successful' options, namely P1-1-QS and P3-3-QS, and 'unsuccessful' options, namely P1-3-QS and P2-3-QS, for the extremely thin beam ($L/h = 10^4$). The shear force diagrams are plotted in Figs. 6(a) and 6(b), respectively. Figure 6(a) shows that the shear force distribution obtained from the K-beam-DSG element with P1-1-QS is, as expected, piecewise constant over each element. This indicates that the element is able to give an optimal approximate solution in the shear strain function space. The shear

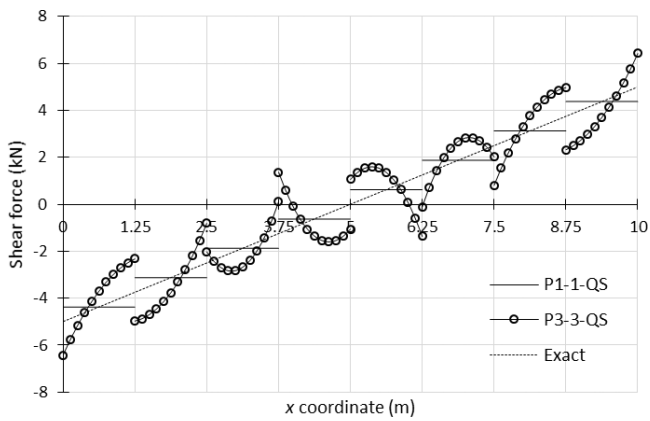

(a)

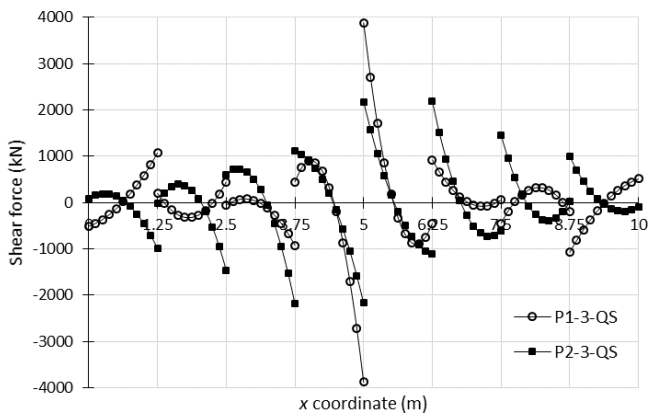

(b)

Fig. 6. Shear force diagram for the clamped–clamped beam with $L/h = 10^4$ obtained using K-beam-DSG elements with options: (a) P1-1-QS and P3-3-QS; (b) P1-3-QS and P2-3-QS.

force distribution corresponding to the P3-3-QS option oscillates about the exact distribution. This oscillation, however, is very mild compared to the violent shear force oscillations obtained from the K-beam-DSG elements with P1-3-QS and P2-3-QS (Fig. 6b). The total area under the shear force curves of P1-1-QS and P3-3-QS seems to be equal to the total area under the exact curve. Furthermore, it was found that with P1-1-QS and P3-3-QS options, the shear force distributions for the beams of L/h greater than 10^4, up to $L/h = 10^7$, remain the same as those for the beam of $L/h = 10^4$. This is in contrast to the oscillation of shear force with the other K-beam element options, which are much heavier as the beams become thinner. This is the reason why the K-beam-DSG elements with P1-1-QS and P3-3-QS options are free of locking while they suffer from shear locking with the other options.

To assess the locking behavior and accuracy of the K-beam-DSG elements in comparison to the original K-beam elements (without any locking treatment) and to the K-beam elements with the selective reduced integration (SRI) technique [Wong and Syamsoeyadi (2011)], the results obtained from a series of analyses using these K-beam elements for the beams with $L/h = 5$ and $L/h = 10{,}000$ are listed in Table 5. It can be seen from Table 5 that without any locking treatment, the K-beam elements suffer from shear locking even for the element with a cubic polynomial basis. The SRI technique is effective at eliminating the locking for all K-beam element options. However, this technique produces less accurate results for the thick beam ($L/h = 5$). The DSG technique produces the most accurate results for the thick beam, but it is only effective at eliminating the shear locking for the K-beam elements with the P1-1-QS and P3-3-QS options.

In the subsequent tests, we only considered the K-beam-DSG element with the P3-3-QS option since this element is free from shear locking and truly Kriging-based finite elements (the element with the P1-1-QS option is essentially identical to the conventional DSG linear beam element [Bletzinger *et al.* (2000)]).

5.1.3. *Assessment of accuracy and convergence*

To assess the accuracy and convergence characteristics of the K-beam element with the P3-3-QS option, we considered a cantilever beam subjected to a linearly varying

Table 5. Normalized deflections obtained using the original and SRI K-beam elements and the K-beam-DSG elements.

	$L/h = 5$			$L/h = 10{,}000$		
K-beam options	Original	SRI	DSG	Original	SRI	DSG
P1-1-QS	0.887	0.958	0.958	1.96E-06	0.938	0.938
P1-2-QS	0.979	1.018	0.999	5.34E-05	1.031	0.003
P1-3-QS	0.983	1.031	0.997	4.33E-04	1.049	0.012
P2-2-QS	0.994	1.001	1.001	5.28E-05	0.999	0.011
P2-3-QS	0.991	1.036	1.003	0.001	1.049	0.010
P3-3-QS	0.999	1.011	1.001	0.002	1.006	1.001

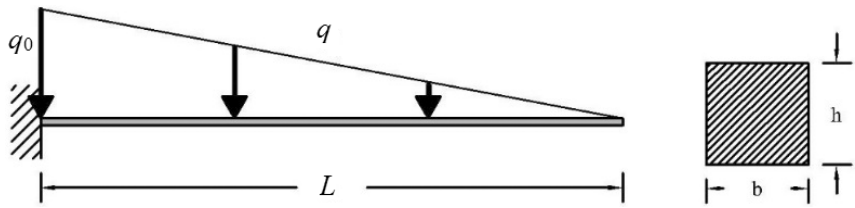

Fig. 7. Cantilever beam subjected to linearly varying load.

distributed load, as illustrated in Fig. 7, under different beam thickness conditions, that is, normal ($L/h = 8$), extremely thick ($L/h = 1$), and extremely thin ($L/h = 10{,}000$). The problem parameters were taken as $L = 4\,\text{m}$, $b = 2\,\text{m}$, $E = 1{,}000\,\text{kN/m}^2$, $v = 0.3$, and $q_0 = 1\,\text{kN/m}$. The beam was analyzed using different degrees of mesh refinement, that is, 4, 8, 16, and 32 elements. The deflection at the free end, the bending moment, and the shear force at the clamped end were observed

Table 6. Results obtained for the normal-thickness beam ($L/h = 8$) using the K-beam P3-3-QS elements with the DSG technique, the SRI technique, and the original element.

Normalized free-end deflection			
	K-beam P3-3-QS		
Number of elements	DSG	SRI	Original
4	0.99989	1.00534	0.99989
8	0.99999	1.00069	0.99999
16	1.00000	1.00017	1.00000
32	1.00000	1.00006	1.00000
Normalized clamped-end bending moment			
	K-beam P3-3-QS		
Number of elements	DSG	SRI	Original
4	0.99972	1.07761	0.92760
8	1.00190	1.04268	0.99075
16	1.00074	1.02153	0.99917
32	1.00022	1.01071	0.99993
Normalized clamped-end shear force			
	K-beam P3-3-QS		
Number of elements	DSG	SRI	Original
4	1.03397	4.25756	1.62985
8	1.00210	1.90156	1.11862
16	1.00022	1.44091	1.01848
32	1.00003	1.34918	1.00251

and normalized to the corresponding exact solutions, viz. [Friedman and Kosmatka (1993)]:

$$w_L = \frac{q_0 L^4}{30EI}\left(1 + \frac{5}{12}\phi\right), \tag{36a}$$

$$\phi = \frac{1}{5}(12 + 11\upsilon)\left(\frac{h}{L}\right)^2, \tag{36b}$$

$$M_0 = \frac{1}{6}q_0 L^2, \quad Q_0 = \frac{1}{2}q_0 L. \tag{37a,b}$$

The results are presented in Tables 6–8 for the normal-thickness, extremely thick, and extremely thin beams, respectively, along with the results obtained using the K-beam P3-3-QS element with the SRI technique and using the original K-beam (without any shear locking treatment). Tables 6 and 7 show that the K-beam-DSG P3-3-QS element can produce remarkably accurate deflection and bending moment and reasonably accurate shear stress, even using relatively course mesh (four elements), for the extremely and moderately thick beams. For the extremely thin beam (Table 8), while the deflection remains very accurate, the accuracy of

Table 7. Results obtained for the extremely thick beam ($L/h = 1$) using the K-beam P3-3-QS elements with the DSG technique, the SRI technique, and the original element.

Normalized free-end deflection			
Number of elements	DSG	SRI	Original
4	0.99995	1.01852	0.99995
8	1.00000	1.00864	1.00000
16	1.00000	1.00359	1.00000
32	1.00000	1.00162	1.00000
Normalized clamped-end bending moment			
Number of elements	DSG	SRI	Original
4	1.00055	1.07761	0.98400
8	1.00192	1.04268	0.99783
16	1.00074	1.02153	0.99974
32	1.00022	1.01071	0.99997
Normalized clamped-end shear force			
Number of elements	DSG	SRI	Original
4	1.00097	1.43572	1.01403
8	1.00019	1.36542	1.00234
16	1.00004	1.33960	1.00034
32	1.00001	1.32864	1.00005

Table 8. Results obtained for the extremely thin beam (L/h = 10,000) using the K-beam P3-3-QS elements with the DSG technique, the SRI technique, and the original element.

Normalized free-end deflection			
Number of elements	DSG	SRI	Original
4	0.99989	1.00486	0.99989
8	0.99999	1.00041	0.99999
16	1.00000	1.00004	1.00000
32	1.00000	1.00001	1.00000
Normalized clamped-end bending moment			
Number of elements	DSG	SRI	Original
4	0.95561	1.07761	0.69987
8	0.95087	1.04268	0.70047
16	0.98499	1.02153	0.72160
32	0.99917	1.01072	0.91343
Normalized clamped-end shear force			
Number of elements	DSG	SRI	Original
4	2.79	4.5E+06	4.7
8	2.59	8.5E+05	16.5
16	0.61	1.6E+05	28.6
32	0.98	3.3E+04	17.6

the bending moment drops a little. The resulting shear stresses, however, are not very accurate for the extremely thin beam.

Tables 6–8 show that all the results converge very well to the corresponding exact solutions. While the SRI technique can eliminate the shear locking, it deteriorates the accuracy in the cases of thick beams (compared to the original K-beam element solutions). Overall, the results of the K-beam-DSG element are better in comparison to those obtained from the original and SRI K-beam elements. Thus, application of the DSG technique to the K-beam elements has improved the elements' performance.

To further demonstrate the accuracy of the K-beam-DSG P3-3-QS element in comparison to the original K-beam P3-3-QS element, the profiles of deflection, rotation, and bending moment for the extremely thin beam case, obtained from the analyses using eight elements, are plotted in Figs. 8(a)–8(c). The shear force profiles obtained from the K-beam-DSG and K-beam elements have not been plotted because they oscillated heavily about the exact shear force. The figures confirm that the K-beam-DSG P3-3-QS element is able to produce accurate results for the deflection, rotation, and bending moment even in the case of the extremely thin beam. The shear force, however, is not accurate. The performance of the element is superior compared to the original K-beam element.

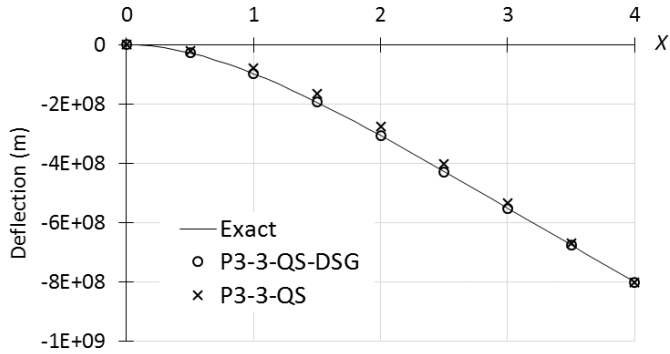

(a) Deflection profile

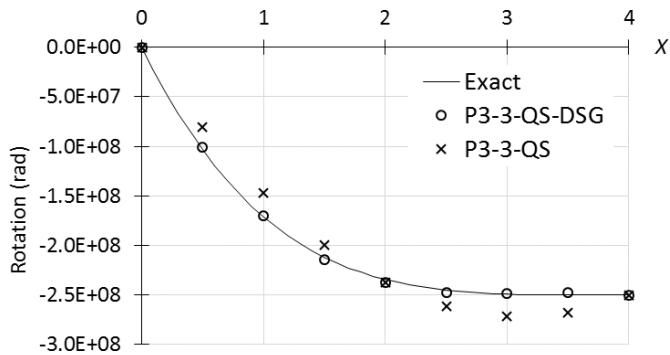

(b) Rotation profile

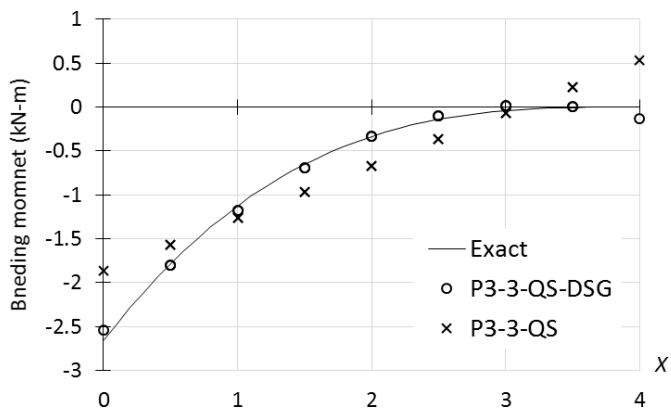

(c) Bending moment profile

Fig. 8. Profiles of (a) deflection, (b) rotation, and (c) bending moment along the extremely thin beam (L/h = 10,000), obtained using the K-beam P3-3-QS element with the DSG technique in comparison to the exact profile and that obtained using the original K-beam P3-3-QS.

5.2. *Free vibration analysis*

5.2.1. *Thick and thin clamped–clamped beams*

To assess the performance of the K-beam-DSG element with the P3-3-QS in free vibration analyses, we first considered free vibration analysis of a clamped–clamped beam with two different thickness conditions, that is, moderately thick ($L/h = 5$) and very thin ($L/h = 1{,}000$). The parameters of the beam were $L = 10\,\text{m}$, $b = 1\,\text{m}$, $E = 2\times10^9\,\text{N/m}^2$, $v = 0.3$, and $\rho = 10\,\text{kg/m}^3$. The beam was modeled using meshes of 4, 8, 16, and 32 elements. The resulting natural frequencies were expressed in the form of dimensionless frequency parameters [Lee and Schultz (2004)], given as

$$\lambda_i = \sqrt{\omega_i L^2 \sqrt{\frac{\rho A}{EI}}}, \tag{38}$$

where ω_i is the natural frequency of the ith vibration mode. The natural frequencies obtained from the pseudo-spectral method [Lee and Schultz (2004)] were taken as the reference solution for the moderately thick beam, while those obtained from the exact solution based on the Euler–Bernoulli beam theory [Lee and Schultz (2004)] were taken as the reference solution for the very thin beam.

The resulting frequency parameters for the first 15 vibration modes obtained using the DSG and original K-beam elements, normalized with respect to the corresponding reference solutions, are presented in Tables 9 and 10 for the moderately thick and very thin beams, respectively. It is seen from Table 9 that for the moderately thick beam, the present K-beam element can give very accurate natural

Table 9. Normalized frequency parameters for the moderately thick beam ($L/h = 5$).

		$\lambda_i/\lambda_i{}^*$							
		4 elements		8 elements		16 elements		32 elements	
Mode shape	λ_i^*	DSG	Original	DSG	Original	DSG	Original	DSG	Original
1	4.2420	1.0039	1.0370	1.0014	1.0180	1.0016	1.0180	1.0016	1.0180
2	6.4188	1.0144	1.1510	1.0021	1.0290	1.0022	1.0280	1.0023	1.0280
3	8.2853	1.1519	1.1940	1.0046	1.0400	1.0027	1.0340	1.0028	1.0340
4	9.9037	1.3579	1.4320	1.0104	1.0550	1.0029	1.0370	1.0031	1.0370
5	11.3847	1.2451	1.3240	1.0223	1.0690	1.0002	1.0370	1.0001	1.0360
6	12.6402	1.2002	1.2650	1.0475	1.0890	1.0042	1.0430	1.0034	1.0420
7	13.4567	—	—	1.0104	1.0610	1.0045	1.0560	1.0044	1.0560
8	13.8101	—	—	1.0461	1.0910	1.0054	1.0460	1.0035	1.0430
9	14.4806	—	—	1.0385	1.0830	1.0041	1.0470	1.0037	1.0470
10	14.9383	—	—	1.0512	1.0900	1.0074	1.0480	1.0036	1.0440
11	15.6996	—	—	1.0753	1.1150	1.0041	1.0410	1.0031	1.0400
12	16.0040	—	—	1.1284	1.1690	1.0107	1.0520	1.0038	1.0460
13	16.9621	—	—	1.1340	1.1710	1.0042	1.0350	1.0025	1.0330
14	16.9999	—	—	1.1963	1.2390	1.0152	1.0570	1.0041	1.0480
15	17.9357	—	—	—	—	1.0203	1.0470	1.0044	1.0440

Note: *Convergent solution from the pseudo-spectral method [Lee and Schultz (2004)].

Table 10. Normalized frequency parameters for the very thin beam ($L/h = 1{,}000$).

		$\lambda_i/\lambda_i{}^*$							
		4 elements		8 elements		16 elements		32 elements	
Mode shape	λ_i^*	DSG	Original	DSG	Original	DSG	Original	DSG	Original
1	4.7300	1.0044	7.5960	1.0012	1.6020	1.0000	1.0280	1.0000	1.0000
2	7.8532	4.2232	12.3080	1.1775	2.1730	1.0017	1.1480	1.0000	1.0040
3	10.9956	12.2361	12.6810	1.7695	4.1300	1.0133	1.3170	1.0000	1.0120
4	14.1372	173.2836	195.6570	2.2220	6.4780	1.0589	1.4490	1.0002	1.0300
5	17.2788	147.5479	160.0830	2.7744	7.9750	1.1689	1.5410	1.0010	1.0560
6	20.4204	129.1803	135.4550	4.0242	8.7380	1.3321	1.8260	1.0030	1.0890
7	23.5619	—	—	8.9171	9.2180	1.4923	2.4440	1.0074	1.1220
8	26.7035	—	—	76.5291	103.5830	1.6049	3.2090	1.0158	1.1520
9	29.8451	—	—	80.4533	92.6800	1.6013	3.9900	1.0298	1.1750
10	32.9867	—	—	75.6397	83.8530	1.5731	4.7140	1.0508	1.1910
11	36.1283	—	—	71.2762	76.5620	1.7623	5.3280	1.0791	1.2050
12	39.2699	—	—	66.7072	70.4380	2.2091	5.8200	1.1138	1.2340
13	42.4115	—	—	61.9115	65.2200	2.9443	6.2270	1.1521	1.3040
14	45.5531	—	—	57.6457	60.7230	4.2292	6.5440	1.1905	1.4360
15	48.6947	—	—	—	—	6.3361	6.6620	1.2253	1.6250

Note: *Exact solution of Euler–Bernoulli beam theory [Lee and Schultz (2004)].

frequencies. Furthermore, the results obtained using the K-beam-DSG element are consistently more accurate than those obtained using the original K-beam. Using only four elements, the DSG K-beam element can predict the first two natural frequencies within 5% accuracy while the original K-beam element can only predict one natural frequency. Using 32 elements, the present element can predict the first 15 natural frequencies with an error of less than 0.5%.

Table 10, however, indicates that the accuracy deteriorates considerably when the beam becomes very thin. Using a mesh of four elements, only the first natural frequency is predicted accurately. Using the same mesh, the original K-beam element gives erroneous results due to shear locking. For this very thin beam, the K-beam-DSG P3-3-QS element needs a mesh of 32 elements to obtain reasonable results for high natural frequencies. As in the case of the thick beam, in this case the performance of the DSG element is also better than that of the original K-beam element.

5.2.2. *Thick simply supported beam*

To assess the performance of the K-beam-DSG P3-3-QS element in comparison to the exact and consistent Timoshenko beam element developed by Friedman and Kosmatka [1993] ('exact' within static analysis), we adopted the beam problem as described in the reference. The problem is a simply supported beam with the parameters $b = 0.2$, $h = 0.2$, $E = 1$, $v = 0.3$, and $L/h = 5$. The first six natural frequencies were calculated using three different meshes, that is, 4, 8, and 20 elements, and then normalized to the first natural frequency based upon the

Table 11. First six normalized natural frequencies of a thick simply supported beam ($L/h = 5$) obtained using the current K-beam-DSG P3-3-QS element and Friedman and Kosmatka element (F&K) [Friedman and Kosmatka (1993)].

		$\omega/\omega_{\mathrm{T}}$					
		4 elements		8 elements		20 elements	
Mode shape	Exact*	Current	F&K	Current	F&K	Current	F&K
1	0.9404	1.0003	1.0024	0.9999	1.0006	1.0001	1.0001
2	3.2672	1.0090	1.0281	0.9996	1.0067	0.9999	1.0010
3	6.2514	1.3180	1.0952	1.0019	1.0241	0.9998	1.0038
4	9.4970	1.8297	1.5101	1.0125	1.0550	0.9997	1.0088
5	12.8357	1.4408	1.4682	1.0446	1.0985	0.9997	1.0161
6	16.1981	1.3535	1.2714	1.0727	1.1371	1.0000	1.0258

Note: *Timoshenko [1922] as cited in Friedman and Kosmatka [1993].

Euler–Bernoulli beam theory, that is,

$$\omega_I = \left(\frac{\pi}{L}\right)^2 \sqrt{\frac{EI}{\rho A}}. \tag{39}$$

The results are presented in Table 11. It can be seen from the table that when only four elements are used, the current element can predict the first two natural frequencies more accurately than the Friedman and Kosmatka element [Friedman and Kosmatka (1993)]. When more elements are used, the current element can predict the first six natural frequencies consistently more accurately than the Friedman and Kosmatka element.

5.3. *Buckling analysis*

To study the accuracy and convergence of the K-beam-DSG P3-3-QS element in predicting the critical buckling load of axially loaded beams, we performed analyses of simply supported and clamped–clamped beams for a variety of beam length-to-thickness ratios, that is, $L/h = 5$, 10, 100, and 1,000, using different meshes of 4, 8, 16, and 32 elements. A comparison is made with the original K-beam P3-3-QS element. The resulting critical loads (Tables 12 and 13) were normalized to the exact solution [Bažant and Cedolin (1991) as cited in Kosmatka (1995)], which accounts for the effect of shear deformation, that is,

$$P_{\mathrm{cr}} = \frac{\pi^2 EI}{L_{\mathrm{eff}}^2}\left(\frac{1}{1+\frac{\pi^2 EI}{L_{\mathrm{eff}}^2 GA_s}}\right), \tag{40}$$

where L_{eff} is the effective length of the beam (L for simply supported beams, $L/2$ for clamped–clamped beams).

It is observed from Tables 12 and 13 that all results converged very well to the corresponding exact solutions. While for the thick beam conditions ($L/h = 5$ and

Table 12. Normalized critical buckling loads of a simply supported beam obtained using the K-beam element with the DSG technique and the original K-beam element.

Number of elements	$L/h = 5$		$L/h = 10$		$L/h = 100$		$L/h = 1{,}000$	
	DSG	Original	DSG	Original	DSG	Original	DSG	Original
4	0.9986	1.0125	0.9985	1.0417	0.9985	1.2072	0.9985	1.2158
8	0.9997	1.0001	0.9997	1.0002	0.9998	1.0094	1.0002	1.1731
16	1.0000	1.0000	1.0000	1.0000	1.0000	1.0002	1.0000	1.0169
32	1.0000	1.0000	1.0000	1.0000	1.0000	1.0000	1.0000	1.0003

Table 13. Normalized critical buckling loads of a clamped–clamped beam obtained using the K-beam element with the DSG technique and the original K-beam element.

Number of elements	$L/h = 5$		$L/h = 10$		$L/h = 100$		$L/h = 1{,}000$	
	DSG	Original	DSG	Original	DSG	Original	DSG	Original
4	1.1254	1.1157	1.1654	1.3451	1.1850	29.9669	1.1852	2891.6
8	0.9972	1.0012	0.9965	1.0029	1.0043	1.0568	1.0612	5.5373
16	0.9997	1.0000	0.9997	1.0001	0.9997	1.0024	1.0028	1.1160
32	1.0000	1.0000	1.0000	1.0000	1.0000	1.0001	1.0000	1.0034

$L/h = 10$) the accuracies of the DSG and original elements are comparable, for the thin beams the performance of the DSG is superior to that obtained using the original element. For the clamped–clamped beam with $L/h = 100$ and $L/h = 1{,}000$ modeled using four elements, the results obtained from the original K-beam element present large errors because of the shear locking.

6. Conclusions

The DSG technique has been applied in the framework of Kriging-based Timoshenko beam elements in an attempt to eliminate shear locking. The essence of the technique is to replace the original kinematic shear strain with a substitute shear strain derived from the interpolation of discrete shear gaps at the nodes in the DOI. The developed elements, referred to as K-beam-DSG elements, were then tested in static, free vibration, and bucking analyses. The results showed that the DSG technique was effective at eliminating the shear locking for the element with a cubic basis function and three element-layer DOI (P3-3-QS) but was not very effective for the other K-FEM options. In all cases, the performance of the K-beam elements was improved by the DSG technique. For a practical range of beam thicknesses, the K-beam-DSG P3-3-QS element can achieve exceptionally accurate defections, rotations, bending moments, natural frequencies, and critical buckling loads and reasonably accurate shear forces with a relatively course mesh. For extremely thin beams, however, the accuracy may deteriorate and the resulting shear force is not accurate with a small number of elements. The application of the DSG technique to the Timoshenko beam model provides understanding and insight regarding its

effectiveness at eliminating shear locking. Future research may be directed to apply the DSG technique to Kriging-based shear deformable plate and shell models.

Acknowledgments

We gratefully acknowledge that this research has been partly supported by the internal research funding of Petra Christian University, Indonesia.

References

Bathe, K. J. [1996] *Finite Element Procedures* (Prentice-Hall, New Jersey).

Bažant, Z. P. and Cedolin, L. [1991] *Stability of Structures*: *Elastic*, *Inelastic*, *Fracture*, *and Damage Theories* (Dover Publications, New York).

Belytschko, T., Lu, Y. Y. and Gu, L. [1994] "Element-free Galerkin methods," *Int. J. Numer. Methods Eng.* **37**, 229–256.

Bischoff, M., Koschnick, F. and Bletzinger, K. [2003] "Stabilized DSG elements — A new paradigm in finite element technology," *Proc. 4th European LS-DYNA Users Conf.*, DYNAmore, Ulm., Retrieved October 27, 2015 from http://www.dynalook.com/european-conf-2003/stabilized-dsg-elements-2013-a-new-paradigm-in.pdf.

Bletzinger, K.-U., Bischoff, M. and Ramm, E. [2000] "A unified approach for shear-locking-free triangular and rectangular shell finite elements," *Comput. Struct.* **75**, 321–334.

Cook, R. D., Malkus, D. S., Plesha, M. E. and Witt, R. J. [2002] *Concepts and Applications of Finite Element Analysis*, 4th Edition (John Wiley and Sons, Madison).

Cowper, G. R. [1966] "The shear coefficient in Timoshenko's beam theory," *J. Appl. Mech.* **33**, 335–340.

Friedman, Z. and Kosmatka, J. B. [1993] "An improved two-node Timoshenko beam finite element," *Comput. Struct.* **47**, 473–481.

Hughes, T. J. R. [1987] *The Finite Element Method*: *Linear Static and Dynamic Finite Element Analysis* (Prentice-Hall, New Jersey).

Kanok-Nukulchai, W., Barry, W., Saran-Yasoontorn, K. and Bouillard, P. H. [2001] "On elimination of shear locking in the element-free Galerkin method," *Int. J. Numer. Methods Eng.* **52**, 705–725.

Koschnick, F., Bischoff, M., Camprubí, N. and Bletzinger, K. U. [2005] "The discrete strain gap method and membrane locking," *Comput. Methods Appl. Mech. Eng.* **194**, 2444–2463.

Kosmatka, J. B. [1995] "An improved two-node finite element for stability and natural frequencies of axial-loaded Timoshenko beams," *Comput. Struct.* **57**, 141–149.

Lee, J. and Schultz, W. W. [2004] "Eigenvalue analysis of Timoshenko beams and axisymmetric Mindlin plates by the pseudospectral method," *J. Sound Vib.* **269**, 609–621.

Liu, G. R. and Quek, S. S. [2003] *The Finite Element Method- A Practical Course* (Butterworth-Heinemann, Oxford).

Nguyen-Thoi, T., Nguyen-Thoi, M. H., Vo-Duy, T. and Nguyen-Minh, N. [2015] "Development of the cell-based smoothed discrete shear gap plate element (CS-FEM-DSG3) using three-node triangles," *Int. J. Comput. Methods* **12**, 1540015.

Nguyen-Thoi, T., Phung-Van, P., Nguyen-Xuan, H. and Thai-Hoang, C. [2012] "A cell-based smoothed discrete shear gap method using triangular elements for static and free vibration analyses of Reissner–Mindlin plates," *Int. J. Numer. Methods Eng.* **91**, 705–741.

Nguyen-Xuan, H., Liu, G. R., Thai-Hoang, C. and Nguyen-Thoi, T. [2010a] "An edge-based smoothed finite element method (ES-FEM) with stabilized discrete shear gap

technique for analysis of Reissner–Mindlin plates," *Comput. Methods Appl. Mech. Eng.* **199**, 471–489.

Nguyen-Xuan, H., Rabczuk, T., Nguyen-Thanh, N., Nguyen-Thoi, T. and Bordas, S. [2010b] "A node-based smoothed finite element method with stabilized discrete shear gap technique for analysis of Reissner–Mindlin plates," *Comput. Mech.* **46**, 679–701.

Olea, R. A. [1999] *Geostatistics for Engineers and Earth Scientistics* (Kluwer Academic Publishers, Boston).

Plengkhom, K. and Kanok-Nukulchai, W. [2005] "An enhancement of finite element method with moving Kriging shape functions," *Int. J. Comput. Methods* **2**, 451–475.

Prathap, G. [1993] *The Finite Element Method in Structural Mechanics* (Kluwer Academic Publishers, Dordrecht).

Prathap, G. [2001] *Finite Element Analysis as Computation*, Retrieved February 5, 2016, from http://www.cmmacs.ernet.in/cmmacs/online_contents.html.

Reddy, J. N. [2006] *An Introduction to the Finite Element Method*, 3rd Edition (McGraw-Hill, Singapore).

Timoshenko, S. P. [1922] "On the transverse vibrations of bars of uniform cross-section," *Philos. Mag. Ser.* 6 **43**, 125–131.

Wackernagel, H. [2003] *Multivariate Geostatistics*, 3rd Edition (Springer, Berlin).

Wong, F. T. [2009] *Kriging-Based Finite Element Method for Analyses of Plates and Shells*, Doctoral dissertation, Asian Institute of Technology, Pathumthani.

Wong, F. T. [2013] "Kriging-based finite element methods for analyses of shear deformable beams and plates," *Proc. 6th Civ. Eng. Conf. Asian Region and Annual HAKI Conference*, paper ID#63. Indonesian Society of Civil and Structural Engineers, Jakarta.

Wong, F. T., Christabel, Y., Pudjisuryadi, P. and Kanok-Nukulchai, W. [2015] "Testing of the Kriging-based finite element to shell structures with varying thickness," *Procedia Eng.* **125**, 843–849.

Wong, F. T. and Kanok-Nukulchai, W. [2006a] "Kriging-based finite element method for analyses of Reissner–Mindlin plates," *Emerging Trends*: *Keynote Lectures and Symposia — Proc. 10th East-Asia Pacific Conf. Struct. Eng. Const.*, Asian Institute of Technology, Bangkok, pp. 509–514.

Wong, F. T. and Kanok-Nukulchai, W. [2006b] "On alleviation of shear locking in the Kriging-based finite element method," *Proc. Int. Civ. Eng. Conf.* "*Towards Sustainable Engineering Practice*," Petra Christian University, Surabaya, pp. 39–47.

Wong, F. T. and Kanok-Nukulchai, W. [2008] "A Kriging-based finite element method for analyses of shell structures," *Proc. 8th World Congr. Comput. Mech. and 5*$^{\text{th}}$ *European Congr. Comput. Methods Appl. Sci. Eng.*, paper a1247, IACM and ECCOMAS, Venice.

Wong, F. T. and Kanok-Nukulchai, W. [2009a] "Kriging-based finite element method: Element-by-element Kriging interpolation," *Civ. Eng. Dimens.* **11**, 15–22.

Wong, F. T. and Kanok-Nukulchai, W. [2009b] "On the convergence of the Kriging-based finite element method," *Int. J. Comput. Methods* **6**, 93–118.

Wong, F. T. and Syamsoeyadi, H. [2011] "Kriging-based timoshenko beam element for static and free vibration analyses," *Civ. Eng. Dimens.* **13**, 42–49.